Desalination and Water Treatment
www.deswater.com

doi: 10.5004/dwt.2017.21102

81 (2017) 303–314
June

Decolorization mechanisms of an anionic dye by using zero-valent iron nanoparticles: application of response surface modeling for the optimization process

Utku Bulut Simsek[a], Meral Turabik[a,b,*]

[a]*Department of Nanotechnology and Advanced Materials, Mersin University, TR-33343, Turkey, Tel. +90 324 361 00 01; emails: mturabik@mersin.edu.tr (M. Turabik), utkubulutsimsek@msn.com (U.B. Simsek)*
[b]*Chemical Program, Technical Science Vocational School, Mersin University, TR-33343, Turkey*

Received 21 February 2017; Accepted 30 June 2017

ABSTRACT

In this study, decolorization of Acid Red 42 (AR 42) by zero-valent iron nanoparticles (nZVI) was investigated in a batch system. Surface composition of nZVI was characterized by scanning electron microscopy, electron dispersive X-ray spectrometer and X-ray diffractogram methods. Three main decolorization mechanism steps that surface reactions including sorption and chemical reaction controlled decolorization of the azo dye were proposed as (i) the cleavage of the azo bonds by reduction of anionic dye, (ii) adsorption of anionic dye on the iron oxides and (iii) decolorization of the azo chromophores by hydrogen peroxide formed in the presence of dissolved oxygen. The response surface methodology was applied in designing the dye removal experiments for evaluating the interactive effects of independent variables and determining the optimum condition. Four independent variables such as nZVI concentration, initial dye concentration, temperature and pH were coded with low and high level and dye removal (%) was obtained as response. The results showed that while the increase in the nZVI concentration and temperature showed positive effects, the increase in pH and initial dye concentration showed negative effect on dye removal efficiency. The interactive effects of whole variables were also investigated.

Keywords: Acid Red 42; Decolorization; Degradation; Optimization; Response surface methodology; Zero-valent iron nanoparticle

1. Introduction

The extensive use of dyes in many applications and high amount of production for different features, colors and forms have generated severe health problems and water pollution in the world [1]. Because of synthetic origin and complex chemical structure, majority of textile dyes are very stable to light and oxidation, highly toxic and their biodegradability by microorganisms is very difficult [2,3]. Besides, dye pollution in receiving water has a lot of serious health problems such as mutations in humans, cancer, dermatitis, skin irritation and allergy [3,4]. To eliminate these hazards, dye wastewaters should be treated before leaving the receiving environment.

A considerable amount of literature has reported the decolorization of dyes by using various materials, but there is still a need to search new materials and methods to increase removal efficiency. In recent years, new nanomaterials have been extensively synthesized and investigated in terms of removal efficiency for contaminants [5]. Zero-valent iron nanoparticles (nZVI) have received most of the attention because of low cost and high reactivity [6,7]. nZVI have a core-shell structure which consists of a metallic iron core and a thin iron oxide shell of a few nanometers. While the iron core serves as an electron source and exerts a reducing character, iron oxide shell surrounds the core and promotes the adsorption of contaminants via electrostatic interactions and surface complexation [8]. As a material, nZVI have been used for the removal/degradation of a wide range of contaminants

---

* Corresponding author.

such as azo dyes, nitro aromatic compounds, halogenated organics, heavy metals, phosphorus, nitrate and toxic inorganic ions [9–14].

The main aims of the present study were to synthesize and investigate the efficiency of nZVI for AR 42 dye removal. AR 42 is an anionic azo dye which is commercially used in the textile industry. More than 50% of all the produced dyes worldwide are azo dyes [15]. Azo dyes generally possess one or more azo bonds (–N=N–) [16], and both the azo dyes and their degradation products (e.g., aromatic amines) are quite toxic and cause mutagenic and carcinogenic effects for organisms and also environmental pollution [15]. Textile industry is one of the largest polluters in the world [3]. Hence, the treatment of textile wastewaters that especially contain azo dyes require well-designed and efficient methods.

Response surface methodology (RSM) is usually used for the experimental design including reduction of variability and improving product and process performance which have a different design method [17]. The Box–Behnken design (BBD) of Design Expert 10.01 program was used for the RSM in the experimental design where each factor takes only three levels. This design is more efficient and economical according to the other 3k designs, especially for a large number of variables [18,19]. In a treatment process, a methodology is needed to identify and optimize the interacting parameters that affect the treatment. Since RSM is a method using for evaluating the simultaneous effect of operating and optimum conditions for desirable responses with less time [20,21], we used this method to optimize and explain the decolorization of an anionic dye, AR 42. So, it is possible to achieve maximum dye removal in real wastewaters by using the BBD combined with RSM and optimization.

2. Material and methods

2.1. Materials

All chemicals were obtained in high purity and used as received, including $FeCl_3$ $6H_2O$ (99%, Merck KGaA, Darmstadt, Germany), $NaBH_4$ (98%, Merck), hexadecyltrimethylammonium bromide (HTAB [99%], Sigma-Aldrich Chemie GmbH, Munich, Germany) and C_2H_5OH (98%, Merck). Acid Red 42 (AR 42, CAS Number 6245-60-9) textile dye was supplied by Dystar Group Singapore Pte Ltd., Singapore, firm and used as received. The characteristics and structures of dye and HTAB are summarized in Table 1.

2.2. Synthesis of HTAB-stabilized zero-valent iron nanoparticles

The synthesis of nZVI was carried out in a batch reactor by the reduction of ferric iron ions with borohydride method with applying an inert atmosphere by using N_2 gases following the process described by Wang and Zhang [22]. While the $FeCl_3$ $6H_2O$ solutions were prepared freshly with absolute ethanol to prevent the oxidation of nZVI, $NaBH_4$ and HTAB solutions were also prepared with ultra-pure water with 18.2 MΩ. The initial concentration of 0.05 M ferric iron and 0.2 M $NaBH_4$ reacted with 1:1 volume ratio of $Fe^{3+} : BH_4$ by using 0.0001 M HTAB as stabilizer.

Because of direct interparticle interactions such as Van der Waals forces and magnetic interactions, agglomeration takes place at magnetic nanoparticles that reduces the specific surface area, interfacial free energy and as result of particle reactivity [23]. If a stabilizer is present in the reaction medium, it gets adsorbed to the surface of particles likely slowing particle growth and blocking certain growth sites on the particles resulting in a layer of negative charges [24].

Table 1
The characteristics and structure of AR 42 and HTAB

Material	Nature	Molecular formula	Structure
Acid Red 42 (AR 42)	Anionic dye	$C_{22}H_{16}N_3NaO_6S_2$	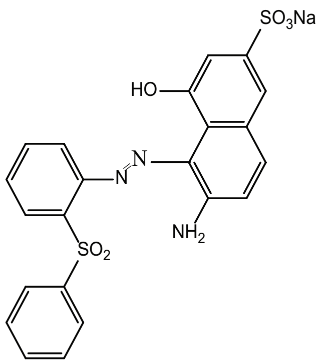
Hegzadecylcetil trimethyl ammonium bromide (HTAB)	Cationic surfactant	$C_{19}H_{42}BrN$	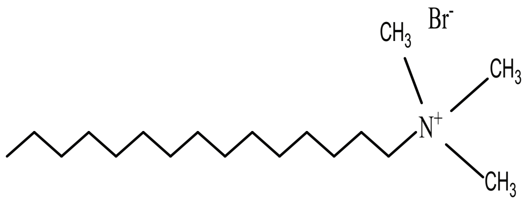

Many stabilizer compounds have been used for the synthesis of nZVI. In this study, HTAB molecules were used as a stabilizer to stabilize the nZVI which is an amine-based cationic quaternary surfactant. Ferric chloride solution was mixed with HTAB solution and agitated for 15 min to produce Fe–HTAB complex. Then the $NaBH_4$ solution was added at 1.0 rpm rate with Longer BT-100J peristaltic pump into the Fe–HTAB complex solution at a vigorous stirring (~400 rpm) and nZVI were synthesized according to following reaction:

$$\begin{aligned}&2FeCl_3 + 6NaBH_4 + 18H_2O \rightarrow 2Fe^0 + 6NaCl\\&\quad + 6B(OH)_3 + 21H_2\end{aligned} \tag{1}$$

After the addition of all $NaBH_4$ solution, the solution was mixed for extra 20 min period. The synthesized black iron nanoparticles were harvested using SIGMA 3-30 K cooling centrifuge at 13,000 rpm. The iron nanoparticles were then washed three times with absolute ethanol, dried at 65°C for 4 h in a vacuum oven and stored in a nitrogen medium for analyses.

2.3. Characterization methods of the nZVI

The scanning electron microscopy (SEM) image and energy dispersive X-ray (EDX) chemical analysis of nanoparticles were recorded with a Zeiss Supra 55VP field emission SEM. The analysis was performed by mounting nZVI samples onto pin type SEM stubs using carbon/platinum adhesive tabs and was coated with carbon/palladium by electro deposition under vacuum prior to analyses to enhance the surface conductivity.

The mean hydrodynamic diameter of the nZVI was determined using dynamic light scattering (DLS). The particles were dispersed in water with Sigma 3-30 K model ultrasound equipment and then measured at 25°C using a Malvern 2000 Zetasizer Nano ZS instrument at an angle of 90° (internal He–Ne laser, wavelength of 633 nm). The analysis of sample was repeated at least six times for 1 mL suspension of sample at 0.1 g Fe^0/L. The DLS data were evaluated with the Malvern Zetasizer 7.1 software package CW380 to yield the volume weighted size distributions that assume the particles to be in spherical shape. Volume distribution is frequently used to determine the modal particle diameter because it contains most of the particle volume. The zero-point charge (pH_{zpc}) of nZVI was also measured with zeta potential measuring by preparing a series of suspensions having adjusted pH values in the range 2–12. The measurements were conducted for 0.1 g/L nZVI concentration using the same apparatus.

X-ray diffractogram (XRD) of nZVI was obtained using a Rigaku SmartLab model XRD at Cu-Kα radiation (λ = 1.54 Å). The analysis of dried nZVI was carried out at continuous scans from 10° to 100° at 2° scan rate at 2θ min^{-1} in ambient air.

Fourier transform infrared spectroscopic (FTIR) analyses of AR 42 dye and nZVI, before and after dye treatment, was recorded using a Perkin-Elmer Model FTIR Frontier spectrophotometer with attenuated total reflection technique in the 4,000–450 cm^{-1} region.

2.4. Preparation of dye solutions and UV–Vis analyses

The stock solutions of AR 42 were prepared in 1.0 g/L concentration and used by diluting with deionized water for further experiments. Before experiments, desired pH of the solution was adjusted by Thermo Scientific Orion 4-Star digital pH meter with diluted H_2SO_4 or NaOH solutions. The UV–Vis spectra of dye solutions were recorded from 200 to 800 nm using a UV–Vis Shimadzu UV1800 Spectrophotometer equipped with a quartz cell of 1.0 cm path length. The concentrations of samples were quantified by measuring the absorption intensity at maximum wavelength.

2.5. Batch experiments

The removal of AR 42 by nZVI was studied in a batch system. After adding a desired amount of nZVI, the solutions were agitated with a thermostatically controlled shaker (Memmert Waterbath WHE-45) for 120 min at ample time. The dye removal efficiency was calculated using the following equation:

$$\text{Removal (\%)} = \left(\frac{C_0 - C_t}{C_0}\right) \times 100 \tag{2}$$

where Removal (%) is dye removal efficiency, C_0 (mg/L) is initial dye concentration, and C_t (mg/L) is the concentration of dye at t min.

2.6. Response surface modeling of variables

RSM was used to determine the optimal set of operational variables in experimental process. The independent variables were coded with low and high level in the BBD that nZVI concentration 0.2–1.5 g/L, initial dye concentration 100–1,000 mg/L, temperature 25°C–55°C and pH 3–10, labeled as A, B, C and D, respectively. The removal percentage of AR 42 was obtained as response $Y_{R(\%)}$ and is given in Table 2.

Optimization processes have been related to chosen factors by the quadratic models. This model is shown as follows:

$$Y_{R(\%)} = \beta_0 + \sum_{I=1}^{k} \beta_i x_i + \sum_{I=1}^{k} \beta_{ii} x_i^2 + \sum_{i=1} \sum_{j=1} \beta_{ij} x_i x_j + \varepsilon \tag{3}$$

where k is the number of factors, x_i and x_j are coded variables; i and j are the index numbers for factor and ε is the residual error; β_0 is the constant coefficient; β_i, β_{ii} and β_{ij} are the first-order, quadratic and interaction effects, respectively [17]. Model fitting and 3D graphical analyses were performed using the Design Expert 10 software. Accuracy of the fit was studied using F-test, p value, correlation coefficient (R^2) and adjusted correlation coefficient (R^2_{adj}).

3. Results and discussion

3.1. Characterization of zero-valent iron nanoparticles

The XRD results of nZVI before and after treatment with AR 42 were given in Fig. 1. The figure indicates that the characteristic basic reflection at 2θ = 44.69° (PDF card number = 01-071-6941) correspond to zero-valent iron (α-Fe) and a small signal for iron oxides at 2θ = 35.63° correspond to oxide layer. The main broad peak belongs to a chemically disordered crystal structured zero-valent state iron. After treatment with dye,

Table 2
Experimental results of BBD

Run	A nZVI concentration (g/L)	B Dye concentration (mg/L)	C T (°C)	D pH	$Y_{R(\%)}$ [AR 42 removal (%)]
1	0.2	300	40	6.5	21.863
2	1.5	300	40	6.5	75.534
3	0.2	1,000	40	6.5	15.081
4	1.5	1,000	40	6.5	63.528
5	0.85	650	25	3	41.709
6	0.85	650	55	3	55.576
7	0.85	650	25	10	45.659
8	0.85	650	55	10	43.441
9	0.2	650	40	3	23.461
10	1.5	650	40	3	68.089
11	0.2	650	40	10	11.301
12	1.5	650	40	10	60.659
13	0.85	300	25	6.5	52.141
14	0.85	1,000	25	6.5	39.176
15	0.85	300	55	6.5	58.895
16	0.85	1,000	55	6.5	37.232
17	0.2	650	25	6.5	16.113
18	1.5	650	25	6.5	59.974
19	0.2	650	55	6.5	9.211
20	1.5	650	55	6.5	63.708
21	0.85	300	40	3	61.365
22	0.85	1,000	40	3	46.022
23	0.85	300	40	10	55.021
24	0.85	1,000	40	10	44.771
25	0.85	650	40	6.5	46.211
26	0.85	650	40	6.5	43.901
27	0.85	650	40	6.5	45.005
28	0.85	650	40	6.5	44.332
29	0.85	650	40	6.5	39.871
30	0.85	650	40	6.5	41.592

additional peaks at about 2θ = 35.60° appear which belong to maghemite (γ-Fe_2O_3, 2θ = 35.68°) and magnetite (Fe_3O_4, 2θ = 35.63°). When nZVI mixed with aqueous dye solution, iron oxide/hydroxides are formed by the oxidation of metal iron nanoparticles [8]. It can therefore be concluded that iron oxides formed during reduction of AR 42 by nZVI in an aqueous solution. These results are supported with the FTIR results.

Fig. 2 shows the particle size distribution (PSD) of the nZVI. The mean diameter (d.nm) of particles was determined as 13.7 nm (100% volume, standard deviation 1.49 d.nm). Thereby, the PSD results showed that synthesized zero-valent iron particles were of nanoscale diameter.

The SEM images of particles indicate that the nZVI are composed of individual, spherical and chain-like structures and also of nanoscale range (Fig. 3). The EDX analysis results also show that the main element is iron, that is, 72.2% (Fig. 4).

The pH_{zpc} of the nZVI is given in Fig. 5. The results indicate that the pH_{zpc} occur at pH 8.3. In literature, pH_{zpc} of nZVI was given in the range of pH_{zpc} 8.0–8.5 depending on the synthesis conditions and stabilizer type. The obtained pH_{zpc} value higher than those of magnetite (Fe_3O_4) (~6.8) and maghemite (γ–Fe_2O_3) (~6.6) [25] imply that the sample is mainly at zero-valent state.

3.2. Analysis of decolorization mechanism with UV–Vis analyses

Acid Red 42 is an azo dye containing two benzene and one naphthalene groups. Fig. 6 illustrates the UV–Vis

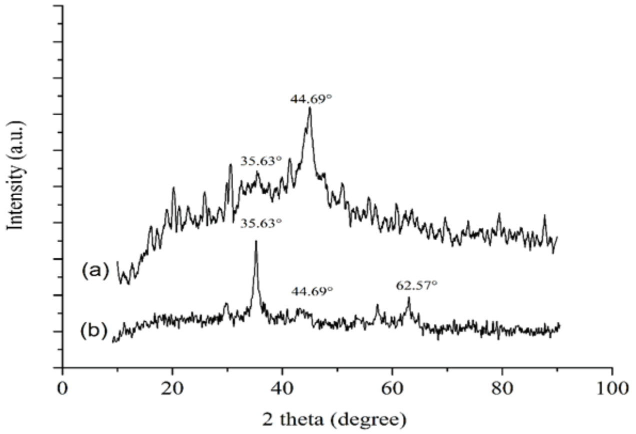

Fig. 1. XRD results of nZVI (a) before reaction with AR 42 and (b) after reaction with AR 42 (nZVI = 0.4 g/L, C_0 = 200 mg/L, pH = 3, T = 37°C).

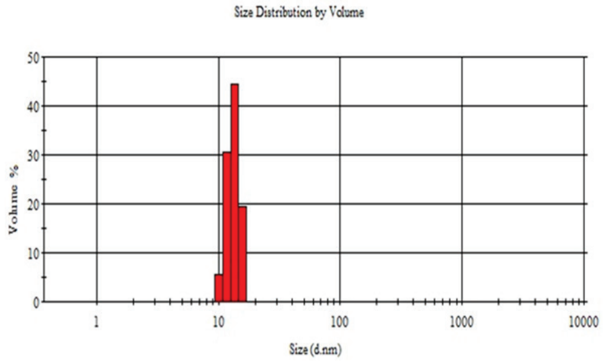

Fig. 2. Particle size distribution of nZVI.

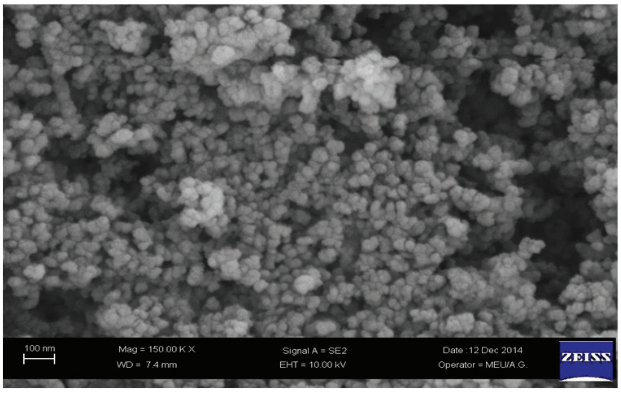

Fig. 3. SEM images of nZVI.

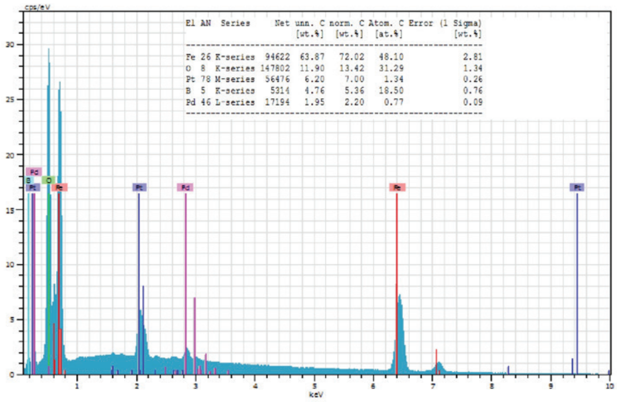

```
El AN  Series     Net unn. C norm. C Atom. C Error (1 Sigma)
                      [wt.%]  [wt.%]  [at.%]           [wt.%]
--------------------------------------------------------------
Fe 26 K-series  94622  63.87   72.02   48.10             2.81
O  8  K-series 147802  11.90   13.42   31.29             1.34
Pt 78 M-series  56476   6.20    7.00    1.34             0.26
B  5  K-series   5314   4.76    5.36   18.50             0.76
Pd 46 L-series  17194   1.95    2.20    0.77             0.09
--------------------------------------------------------------
```

Fig. 4. EDX results of nZVI.

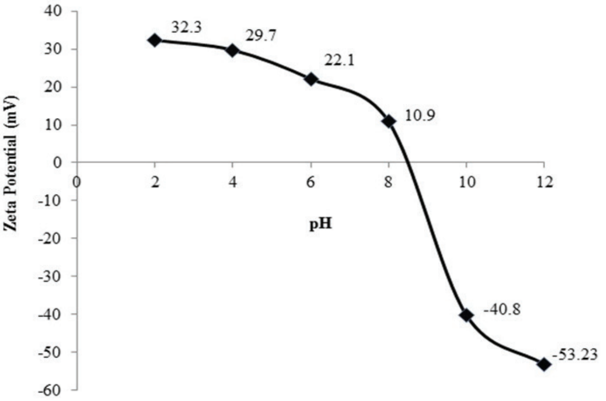

Fig. 5. Zeta potential of nZVI.

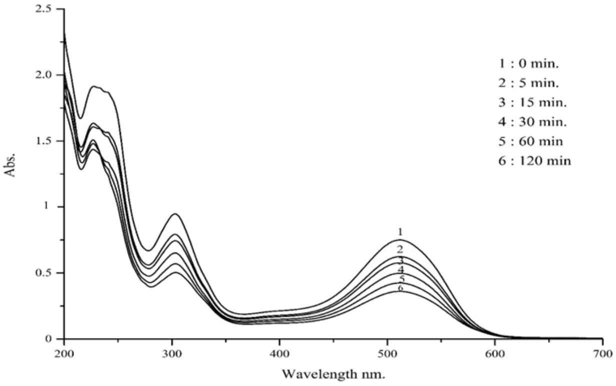

Fig. 6. The UV–Vis spectra of AR 42 obtained before and after treatment by nZVI at different time for 40 mg/L of initial dye concentration.

spectra of dye obtained before and after treatment with nZVI at different treatment time. It is seen that AR 42 has four absorbance peaks at 230, 242, 306 and 514 nm. The intensity of the all peaks was decreased with time after treatment. The observed strong absorbance peak at λ_{max} = 514 nm belongs to the azo bonds that the intensity of this peak implies dye concentration in the solution. The other three bands at 230, 306 and 242 nm in the ultraviolet region are ascribed to the benzene, naphthalene rings and $-NH_2$ groups, respectively [26]. It was observed that no new peak appeared but the peak at λ_{max} became weaker with time that shows the cleavage of the azo bonds, and also $-NH_2$ group peak observed at 242 nm decreased and expanded with time. These results showed decomposition of AR 42 in the solution.

3.3. Analysis of decolorization mechanism with FTIR

To examine the degradation in detail, FTIR analyses of AR 42 were performed both in solid and solution forms. The FTIR spectra of nZVI and AR 42 dye, before and after treatment with nZVI were obtained in the range of 4,000–450 cm^{-1} (Fig. 7(a)–(b)). The spectra obtained in solid forms showed that by the nZVI interaction with AR 42, degradation took place. Fig. 7(a) shows that the band around 1,445 cm^{-1} representing azo bond (N=N) and the benzene ring (at 1,400–1,600 cm^{-1}) [27,28] of AR 42 became weaker and disappeared which is the evidence of the degradation resulting in decolorization. Also, the structure of aromatic ring between 670 and 870 cm^{-1} existing in the dye was broken, which was supported by the absence of the characterized bands [28]. The intensity of band at 1,032 cm^{-1} meaning $C–NH_2$ became weaker in the AR 42 treated nZVI spectrum that this result was supported by the UV–Vis spectrum of dye after treatment with nZVI (Fig. 6). The broad band observed at 3,300 cm^{-1} which was due to –OH stretching was also observed both before and after treatment [28]. The characteristic peaks at 1,143 and 1,032 cm^{-1}, attributed to the asymmetric stretching vibration of the $–SO_3Na$ group [29] also clearly decreased and disappeared, respectively [27].

In addition, when nZVI alone and nZVI after treated with AR 42 spectra were compared, the bands at 796, 991 and 1,035 cm^{-1} corresponding to the FeAO stretch regarding Fe_2O_3 and Fe_3O_4 were observed which supported the XRD results (Figs. 1 and 7) [30]. Similar changes were also observed in FTIR spectra of AR 42 by using solution form of dye (Fig. 7(b)).

As a conclusion, FTIR results showed that decolorization of AR 42 was confirmed by the cleavage of azo bond and dye molecule was transformed into lower molecular weight compound.

3.4. Decolorization reaction mechanisms of an anionic dye AR 42

Decolorization mechanism of AR 42 dye in aqueous solution using nZVI can be summarized in three different ways [23,29,31]:

(i) AR 42 dye is reduced by nZVI to –3 charges and also Fe^0 is oxidized to Fe^{2+} in different ways (Eqs. (4)–(7)):

$$Fe^0 + (AR42)^- \rightarrow Fe^{2+} + (AR42)^{3-} \tag{4}$$

$$Fe^0 + 2H_2O \rightarrow Fe^{2+} + H^+ + OH^- + 2e^- \tag{5}$$

$$Fe^0 + H^+ \rightarrow Fe^{2+} + H^\bullet \tag{6}$$

$$Fe^0 + 2H^+ \rightarrow Fe^{2+} + H_2\uparrow \tag{7}$$

While nZVI directly react with dye molecules, it is oxidized and dye molecules are reduced. By the reaction of Fe^0 with H_2O or H^+, H atoms and of $H^\bullet$ radicals are generated. With the oxidation of Fe^0 to Fe^{2+}, the chromophore groups and conjugated systems of anionic dye are destroyed which leads to the decolorization of dye (Eqs. (8) and (9)) [32,33]:

$$R_1 - N = N - R_2 + 2H^+ + 2e \rightarrow R_1 - NH + HN - R_2 \tag{8}$$

$$R_1 - N = N - R_2 + H^\bullet \rightarrow R_1 - NH + HN - R_2 \tag{9}$$

The generated $H^\bullet$ radicals in an acid solution cleave the azo bond (–N=N–) and consequently the visible absorption peaks at 514 nm corresponding to azo bond decreases with time [34].

(ii) The adsorption of dye and intermediate product on the Fe^0 (Fe^{2+}, Fe^{3+}) [8,23]:

$$Fe^{2+} \rightarrow Fe^{3+} + e^- \tag{10}$$

$$Fe^{3+} + 3OH^- \rightarrow Fe(OH)_3 \rightarrow FeOOH + H_2O \tag{11}$$

$$\begin{aligned} &Dye + Fe_3O_4 / \gamma\text{-}Fe_2O_3 \rightarrow Dye - Fe_3O_4 / \gamma\text{-}Fe_2O_3 \\ &\quad \text{(adsorption)} \end{aligned} \tag{12}$$

By the oxidation of nZVI with oxygen in solution, iron oxides at different forms (Fe_3O_4, Fe_2O_3, $Fe(OH)_3$ and

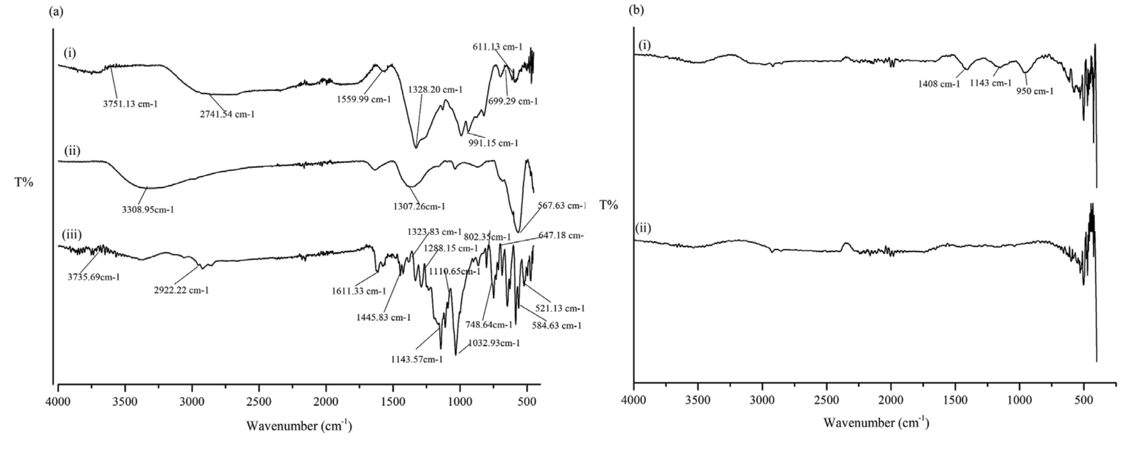

Fig. 7. (a) FTIR spectra of solid (i) nZVI (ii) nZVI after treatment with AR 42 (iii) AR 42 (nZVI = 0.4 g/L, C_0 = 200 mg/L, pH = 3, T = 37°C). (b) FTIR spectra of solution (i) AR 42 (ii) AR 42 after treatment with nZVI (nZVI = 0.4 g/L, C_0 = 200 mg/L, pH = 3, T = 37°C).

FeOOH) are produced at the surface of the particles as confirmed by XRD [30,35]. Dye molecules can be adsorbed by the formed passive iron oxides layers via the sulfonic group causing decolorization of the dye wastewater (Eqs. (10)–(12)) (34,36).

(iii) Producing hydrogen peroxide in reaction medium.

Although Fe^0 is a mild reductant ($E^0_{\text{reduction}} = -0.44$, vs. standard hydrogen electrode) under the anoxic condition [31] but in the presence of dissolved oxygen, iron corrosion can generate hydrogen peroxide (Eq. (13)). Hydrogen peroxide may also be produced by the reaction of ferrous iron and oxygen (Eq. (14)) [37]. Subsequently hydrogen peroxide and ferrous iron act as Fenton system that they can react with the Fe^{2+} (Eq. (15)) to produce a strong oxidant, hydroxyl radical ($OH\bullet$) which can decolorize the azo chromophore. In this system Fe^{3+} can be reduced to Fe^{2+} by Fe^0 (Eq. (17)) allowing a fast recycling of Fe^{3+} [32,37]:

$$\mathrm{Fe^0 + O_2 + 2H^+ \rightarrow H_2O_2 + Fe^{2+}} \tag{13}$$

$$\mathrm{2Fe^{2+} + O_2 + 2H^+ \rightarrow 2Fe^{3+} + H_2O_2} \tag{14}$$

$$\mathrm{Fe^{2+} + H_2O_2 \rightarrow Fe^{3+} + OH^\bullet + OH^-} \tag{15}$$

$$\mathrm{2Fe^{3+} + Fe^0 \rightarrow 3Fe^{2+}} \tag{16}$$

$$\mathrm{Dye + OH^\bullet \rightarrow oxidized\ dye + CO_2 + H_2O} \tag{17}$$

The two research works of Chang et al. also showed that decolorization extent of two anionic azo dyes, Reactive Black 5 [32] and Acid Black 1 [33] was much higher by the Fe^0/air process than the Fe^0/N_2 process because of the formed strong oxidant. For this study, it is possible to say that the dye solution and nZVI can interact with oxygen from the air and aqueous medium containing dissolved oxygen. This third step, strong oxidant effect is also one of the possible mechanisms for decolorization. Thus, it can be concluded that surface reactions including sorption and chemical reaction controlled decolorization of the azo dye.

3.5. Assessment of experimental design with design expert software

Four independent process variables such as nZVI concentration (A), initial dye concentration (B), temperature (C) and pH (D) were defined to investigate their effect on decolorization. To calculate the number of required experiments, following formula is used:

$$N = 2k(k-1) + C_p \tag{18}$$

where k is the number of factors and C_p is the number of central points. For these factors, a set of 30 experiments is required to optimize the removal percentage of AR 42 as shown in Table 2.

The individual and interactive effects of the set four independent variables on the removal % of dye in an aqueous solution were investigated using the BBD application with RSM and obtained results were given in Table 3. The experimental data evaluated with RSM of Design-Expert 10.01 showed that quadratic polynomial regression model was statistically significant because of the calculated F-value = 72.54 with a very low probability value ($p < 0.0001$). If the model has a high degree of adequacy to predict the experimental results, it is expected that the computed F-value should be greater than the tabulated F-value at a level of significance α. Thus, when the tabulated F-value ($F_{0.05,\text{df},(n-(\text{df}+1))}$ $\alpha = 0.05$, degrees of freedom value is 14 and $n = 30$) is compared with calculated F-value, ($F_{\text{model}} = 72.54$) it is seen that the tabulated F-value ($F_{0.05,14,15} = 2.48$) is clearly less than calculated F-value [38].

The quality of fit of the quadratic model was also expressed by the determination of R^2 and R^2_{adj} values. The correlation coefficient, R^2, explains the correlation between the experimental data and predicted responses, and also the adjusted coefficient R^2_{adj} is suitable to compare the models with different numbers of independent variables. The obtained values of R^2 and R^2_{adj} from model were found as 0.930 and 0.972, respectively. As indicated in Fig. 8(a), R^2 regression line between the experimental and model predicted values of the response variable showed the excellent fit of the model. A plot of the normal probability of the residuals is shown in Fig. 8(b). According to this figure, the residuals trends line fits to normal range. In addition, trend of residuals to a normal distribution where the errors are normally distributed and independent of each other is shown at Fig. 8(b) and also error variance is homogenous. Furthermore, the 'Adequate precision' value which is the measure of the signal-to-noise ratio obtained as 31.51 indicates that for an adequate signal the value should be greater than 4. It is seen that model signal is in adequate amount in order to better design on the space. These statistical parameters are approximately close to one, there is relatively good agreement between the experimental and predicted value.

Fig. 8(c) shows a plot of residuals vs. predicted response that provides handy diagnosis for non-constant variance. Also shows that the fitted value and residuals for all predicted data are in the reliable range. The normal plot of standardized residual vs. experimental run number is given in Fig. 8(d). By using this plot lurking variable can be checked that may have influenced the response during the experiment. The plot should show a random scatter around the center line in the interval of ±4.00. These trends indicate that time related lurking variable in the background of the plot. There have not been explicit deviation at the observation order (±4.00). Furthermore, all the values lie within the range of –3 and +3 being acceptable limits.

The approximating functions of the AR 42 removal percentage $Y_{R(\%)}$ in terms of the coded variables obtained are shown as follows:

$$\begin{aligned} \mathrm{Y_{R(\%)}} &= 43.49 + 24.54\mathrm{A} - 6.58\mathrm{B} + 1.11\mathrm{C} - 2.95\mathrm{D} - 1.31\mathrm{AB} \\ &\quad + 2.66\mathrm{AC} + 1.18\mathrm{AD} - 2.17\mathrm{BC} + 1.27\mathrm{BD} - 4.02\mathrm{CD} \\ &\quad - 5.24\mathrm{A}^2 + 5.02\mathrm{B}^2 - 0.95\mathrm{C}^2 + 3.33\mathrm{D}^2 \end{aligned} \tag{19}$$

Pareto analyses have given more information about significance level of variables and also single or synergistic positive or antagonistic effects of variables on the studied response. The following formula was used for the

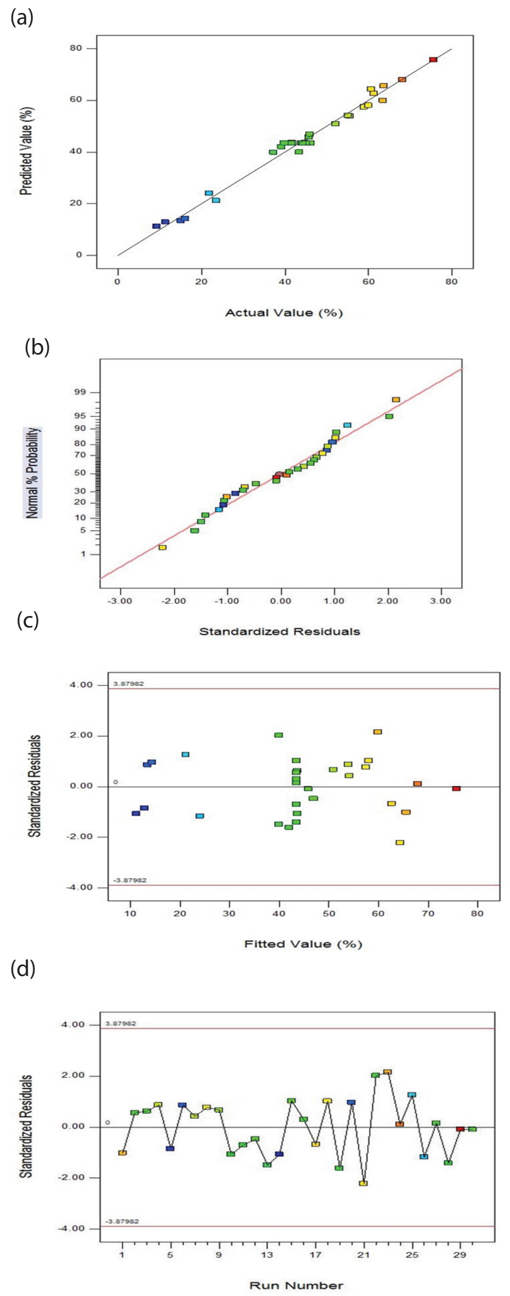

Fig. 8. (a) The actual and predicted plot of AR 42 removal percentage (R^2 = 0.930, R^2_{adj} = 0.972). (b) The standardized residual and normal% probability plot of AR 42 removal percentage. (c) The fitted value (%) and standardized residual plot of AR 42 removal. (d) The standardized residuals plot of AR 42 removal.

significance of each factor, the percentage effect of each term on the response [39,40]:

$$P_i = \left(\frac{\beta_i^2}{\sum \beta_i^2}\right) \times 100\ (i \neq 0) \tag{20}$$

where P_i is the percentage effect of each factor and β_i is the corresponding coefficient. According to Pareto analyses, the effect of nZVI concentration (94.32%) and initial dye concentration (6.79%) are more effective parameters than temperature (0.19%) and pH (1.36%) for the removal of AR 42 (Fig. 9). The interactive effects of these independent variables were also effective for dye decolorization. A positive sign of the interactive coefficients of the nZVI concentration–temperature, nZVI concentration–pH and initial dye concentration–pH systems indicated synergistic effect on removal efficiency, while interaction between the nZVI concentration–initial dye concentration, initial dye concentration–temperature and temperature–pH showed antagonistic effect. Sohrabi et al. [41] indicated that the optimization of Direct yellow 12 anionic dye removal by using zero-valent iron nanoparticles fits the quadratic polynomial model. Furthermore, independent variables of Pareto analyses show that nZVI dosage, pH and initial dye concentration were important parameters and removal percentage of this dye was 90.02% [41].

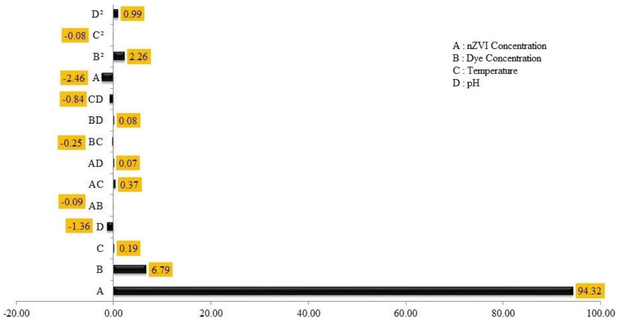

Fig. 9. Graphical Pareto analyses for AR 42 removal.

RSM has also been used to optimize the removal of heavy metals by using nZVI in a wide range. Gholinezhad et al. [42] have worked response surface modeling and optimization of chromium removal from aqueous solution using nZVI and they reported that nZVI dosage is the most important parameter. Fan et al. [43] also investigated the removal optimization of Pb(II) by using reduced graphene oxide–supported nZVI by applying BBD and they reported that design fit of the quadratic polynomial model and also according to Pareto analyses, temperature, pH and nZVI concentration are important parameters.

3.6. Effects of variables in the three-dimensional response surface plots

The three-dimensional response plots for the four variables were used to obtain the relationship between each other on the percentage of removal efficiency, organized based on quadratic polynomial model and results were presented in Figs. 10(a)–(f).

Fig. 10(a) shows that when the initial dye concentration decreases, the efficiency of dye removal increases. For example, when the initial dye concentration was decreased from 350 to 300 g/L and also nZVI concentration was increased from 1.2 to 1.5 g/L, removal percentage improved from 60% to 85% at pH 3 and 46°C. Because of the low active sites, surface relation to high dye concentration removal value is low. On the other hand, as the nZVI concentration increases there has been high active sites available so all dye molecules stick to nZVI surface thus the efficiency of removal increases.

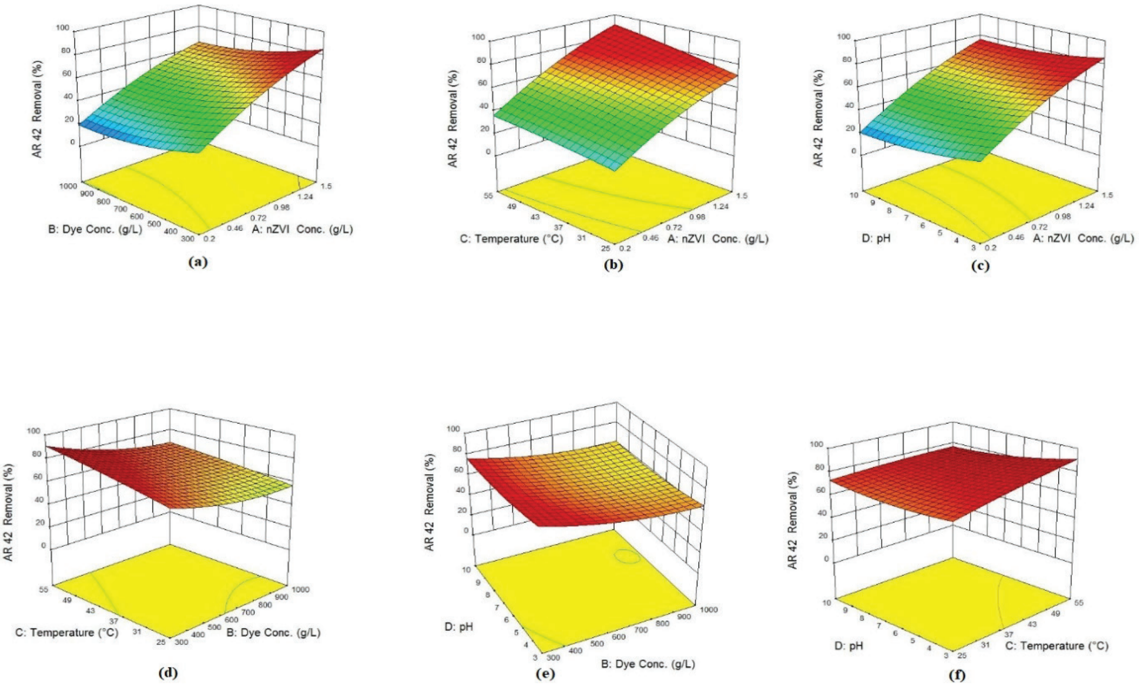

Fig. 10. Three-dimensional surface plots based on BBD showing the interaction effects of (a) nZVI concentration and initial dye concentration (T = 46°C, pH 3), (b) nZVI concentration and temperature (C_0 = 300 g/L, pH 3), (c) nZVI concentration and pH (C_0 = 300 g/L, T = 46°C), (d) temperature and initial dye concentration (nZVI = 1.5 g/L, pH 3), (e) initial dye concentration and pH (T = 46°C, nZVI = 1.5 g/L) and (f) pH and temperature (C_0 = 300 g/L, nZVI = 1.5 g/L).

The interaction effect of temperature and nZVI concentration is synergistic. Fig. 10(b) shows that when the nZVI concentration and temperature values increase from 0.58 to 1.5 g/L and from 35°C to 43°C, removal efficiency of AR 42 increases from 48.75% to 81.25%, respectively. Fig. 10(c) also demonstrates the interaction effect of nZVI and pH. Whenever pH decreases along with an nZVI concentration increase, the removal efficiency of AR 42 increases. For example, when pH decreases from 10 to 3 and also nZVI concentration increases from 0.2 to 1.5 g/L, removal improves from 44.38% to 85.24%. The initial dye concentration and temperature effect on removal efficiency was also investigated. It is seen in Fig. 10(d) that low initial dye concentration and high temperature conditions were effective parameters for AR 42 dye removal. When the initial dye concentration decreases from 500 to 300 g/L and also temperature increases from 37°C to 43°C, the removal efficiency of AR 42 increases from 58.71% to 83.35%.

The ionization state of nanoparticles surface is affected by the pH value of the aqueous solution [26]. The obtained results showed that the degradation of AR 42 was pH dependent, with increase in pH value, the removal % values gradually decreased. Fig. 10(e) clearly indicates that as the pH decrease from 8 to 3 and initial dye concentration decreases from 600 to 300 mg/L, the removal efficiency improves from 51.33% to 72.75%. By the reduction reaction in the acidic solutions hydrogen gas is produced which attacks azo bond of dye molecules and reduces it to hydrogenated azo bond structure (Eqs. (8) and (9)) [14,44]. According to reduction potential of nZVI in acidic and basic medium, the AR 42 reaction with nZVI can be written as [32,45]:

$$\mathrm{Fe}^0 + (\mathrm{AR42})^{2-} \rightarrow \mathrm{Fe}^{2+} + (\mathrm{AR42})^{-4} \qquad (\mathrm{pH} < 6) \tag{21}$$

$$(\mathrm{AR42})^{2-} + \mathrm{FeOH} \rightarrow \mathrm{FeOH(AR42)}^{-} \qquad (\mathrm{pH} > 6) \tag{22}$$

The decline in the degradation of dye at higher pH resulted from two processes. First, the oxide surface becoming negatively charged if the solution pH higher than the $\mathrm{pH_{zpc}}$, led to repulsion of anionic dye. The nZVI's $\mathrm{pH_{zpc}}$ was found to be 8.5 (Fig. 5). Second, ferrous ions and ferric iron were produced by corrosion of Fe^0 in an aqueous solution but precipitated as hydroxides at higher pH, which covered the surface of Fe^0 and thus retarded the reaction [46,47].

Usually temperature is one of the main parameter effecting the chemical reaction and providing some insight into the reaction mechanism [37]. Fig. 10(f) shows the interaction effect of temperature and pH. When temperature increases from 37°C to 45.7°C and pH decreases from 10 to 3, the removal efficiency is improved from 38.2% to 78.75%. The improved efficiency at high temperature is due to the increasing mobility of dye from the solution to nanoparticles' surface and molecular kinetic energy increases as the temperature rises that the decolorization was improved by the acceleration of degradation [36,48].

According to model optimization (Figs. 10(a)–(f)), three optimal experimental conditions were determined and proposed for the most AR 42 removal % and the results were numbered as 1, 2 and 3, respectively, as given in Table 4.

Table 3
ANOVA results of quadratic model

Source	Sum of squares	df	Mean square	F value	*p* value Probability > F
Model	8,509.27	14	607.81	72.54	<0.0001
A-nZVI concentration	7,225.66	1	7,225.66	862.39	<0.0001
B-dye concentration	520.20	1	520.20	62.09	<0.0001
C-temperature	14.72	1	14.72	1.76	0.2048
D-pH	104.25	1	104.25	12.44	0.0030
AB	6.82	1	6.82	0.81	0.3811
AC	28.28	1	28.28	3.38	0.0861
AD	5.59	1	5.59	0.67	0.4267
BC	18.91	1	18.91	2.26	0.1537
BD	6.48	1	6.48	0.77	0.3929
CD	64.68	1	64.68	7.72	0.0141
A^2	188.36	1	188.36	22.48	0.0003
B^2	172.95	1	172.95	20.64	0.0004
C^2	6.22	1	6.22	0.74	0.4026
D^2	75.94	1	75.94	9.06	0.0088
Residual	125.68	15	8.38		
Lack of fit	98.40	10	9.84	1.80	0.2673
Pure error	27.28	5	5.46		
Corrected total	8,634.95	29			
Standard deviation	2.89	R^2	0.986		
Mean	44.35	Adjusted R^2	0.972		
C.V.%	6.53	Predicted R^2	0.930		
PRESS	606.08	Adequate precision	31.509		

Table 4
Optimum conditions derived by BBD

Number	nZVI Conc. (g/L)	Dye conc. (mg/L)	Temperature (°C)	pH	AR 42 Removal (%)	Desirability
1	*1.50*	*301.09*	*45.86*	*3.16*	*85.24*	*1.000*
2	1.48	301.70	45.84	3.10	85.06	1.000
3	1.50	343.76	46.00	3.05	83.31	0.661

The highest removal % of AR 42 was obtained as 85.24% at 1.5 g/L nZVI concentration, 301.09 mg/L initial dye concentration, pH 3.16 and 45.86°C temperature condition as indicated in italics in Table 4. As a result, the application of the BBD combined with the response surface modeling and optimization will help to achieve the optimal solution of reaching the maximum dye removal in real wastewaters by using nZVI.

4. Conclusion

nZVI were synthesized with mean particle diameter of 13.7 nm and used for the decolorization of Acid Red 42. The XRD results of nZVI showed that the main material was zero-valent iron, after treatment of nZVI with dye, the iron oxide forms were also determined. The results of UV–Vis and FTIR spectra showed that decolorization of AR 42 was confirmed by the cleavage of azo bond of the molecule. Three main steps were proposed for the decolorization mechanism of AR 42 by using nZVI: (i) the cleavage of the azo bonds by reduction of anionic dye/oxidation of Fe^0, (ii) adsorption of anionic dye on the iron oxides, (iii) hydrogen peroxide formed in the presence of dissolved oxygen that is a strong oxidant decolorized the azo chromophores.

RSM was applied in designing the dye removal experiments with low and high level of independent variables such as nZVI concentration, initial dye concentration, temperature and pH and dye removal % was also obtained as response. The high F, R^2 and R^2_{adj} value are 72.54, 0.930 and 0.972, respectively, showed that the quadratic polynomial model was suitable for modeling of the decolorization process. According to Pareto analyses, nZVI and initial dye concentration were the most effective parameters. The interactive effects of these independent variables were also effective for AR 42 dye decolorization. As a result, the optimum conditions for AR 42 removal % was determined as 1.5 g/L nZVI concentration, 301.09 g/L initial dye concentration, pH 3 and 45.86°C temperature. According to the optimum conditions mentioned, the maximum AR 42 removal % is 85.24%.

Acknowledgments

This study was supported by Mersin University Scientific Research Foundation (Contract Number: BAP-FBE KTB (UBŞ) 2014-2 YL).

References

[1] U.A. Isah, G. Abdulraheem, S. Bala, S. Muhammad, M. Abdullahi, Kinetics, equilibrium and thermodynamics studies of C.I. Reactive Blue 19 dye adsorption on coconut shell based activated carbon, Int. Biodeterior. Biodegrad., 102 (2015) 265–273.

[2] V.S. Mane, P.V. Vijay Babu, Kinetic and equilibrium studies on the removal of Congo red from aqueous solution using Eucalyptus wood (*Eucalyptus globulus*) saw dust, J. Taiwan Inst. Chem. Eng., 44 (2013) 81–88.

[3] C. Djilani, R. Zaghdoudi, F. Djazi, B. Bouchekima, A. Lallam, A. Modarressi, M. Rogalski, Adsorption of dyes on activated carbon prepared from apricot stones and commercial activated carbon, J. Taiwan Inst. Chem. Eng., 53 (2015) 112–121.

[4] K.G. Bhattacharyya, A. Sharma, *Azadirachta indica* leaf powder as an effective biosorbent for dyes: a case study with aqueous Congo Red solutions, J. Environ. Manage., 71 (2004) 217–229.

[5] Y.R. Zhang, S.L. Shen, S.Q. Wang, J. Huang, P. Su, Q.R. Wang, B.X. Zhao, A dual function magnetic nanomaterial modified with lysine for removal of organic dyes from water solution, Chem. Eng. J., 239 (2014) 250–256.

[6] L. Chekli, B. Bayatsarmadi, R. Sekine, B. Sarkar, A.M. Shen, K.G. Scheckel, W. Skinner, R. Naidu, H.K. Shon, E. Lombi, E. Donner, Analytical characterisation of nanoscale zero-valent iron: a methodological review, Anal. Chim. Acta, 903 (2016) 13–35.

[7] Y. Dai, Y. Hu, B. Jiang, J. Zou, G. Tian, H. Fu, Carbothermal synthesis of ordered mesoporous carbon-supported nano zero-valent iron with enhanced stability and activity for hexavalent chromium reduction, J. Hazard. Mater., 309 (2016) 249–258.

[8] A. Liu, J. Liu, J. Han, W. Zhang, Evolution of nanoscale zero-valent iron (nZVI) in water: microscopic and spectroscopic evidence on the formation of nano- and micro-structured iron oxides, J. Hazard. Mater., 322 (2017) 129–135.

[9] O. Eljamal, A.M.E. Khalil, Y. Sugihara, N. Matsunaga, Phosphorus removal from aqueous solution by nanoscale zero valent iron in the presence of copper chloride, Chem. Eng. J., 293 (2016) 225–231.

[10] Z. Jiang, S. Zhang, B. Pan, W. Wang, X. Wang, L. Lv, W. Zhang, Q. Zhang, A fabrication strategy for nanosized zero valent iron (nZVI)-polymeric anion exchanger composites with tunable structure for nitrate reduction, J. Hazard. Mater., 6 (2012) 233–234.

[11] S. Wang, B. Gao, Y. Li, A.E. Creamer, F. He, Adsorptive removal of arsenate from aqueous solutions by biochar supported zero-valent iron nanocomposite: batch and continuous flow tests, J. Hazard. Mater., 322 (2017) 172–181.

[12] Y. Lv, Z. Zhang, Y. Chen, Y. Hu, A novel three-stage hybrid nano bimetallic reduction/oxidation/biodegradation treatment for remediation of 2,2′4,4′-tetrabromodiphenyl ether, Chem. Eng. J., 289 (2016) 382–390.

[13] S. Nam, P.G. Tratnyek, Reduction of azo dyes with zero-valent iron, Water Res., 34 (2000) 1837–1845.

[14] J. Yang, M. Zhu, X. Wang, P.J.J. Alvarez, K. Liu, Poly(vinylidene fluoride) membrane supported nano zero-valent iron for metronidazole removal: influences of calcium and bicarbonate ions, J. Taiwan Inst. Chem. Eng., 49 (2015) 113–118.

[15] A.B. Volikov, S.A. Ponomarenko, A.I. Konstantinov, K. Hatfield, I.V. Perminova, Nature-like solution for removal of direct brown 1 azo dye from aqueous phase using humics-modified silica gel, Chemosphere, 145 (2016) 83–88.

[16] B. Heibati, S. Rodriguez-Couto, M.A. Al-Ghouti, M. Asif, I. Tyagi, S. Agarwal, V.K. Gupta, Kinetics and thermodynamics of enhanced adsorption of the dye AR 18 using activated carbons prepared from walnut and poplar woods, J. Mol. Liq., 208 (2015) 99–105.

[17] C. Dougla, C.R.H.M. Montgomery, Response Surface Methodology: Process and Product Optimization Using Designed Experiments, Wiley, USA, 2009.

[18] B. Gozmen, O. Sonmez, M. Turabik, Basic Yellow 28 Dye by temperature and ferrous ion activated persulfate, Asian J. Chem., 25 (2013) 6831–6839.

[19] M.A. Bezerra, R.E. Santelli, E.P. Oliveira, L.S. Villar, L.A. Escaleira, Response surface methodology (RSM) as a tool for optimization in analytical chemistry, Talanta, 76 (2008) 965–977.

[20] M.M. Song, C. Branford-White, H.L. Nie, L.M. Zhu, Optimization of adsorption conditions of BSA on thermosensitive magnetic composite particles using response surface methodology, Colloids Surf., B, 84 (2011) 477–483.

[21] S.S. Moghaddam, M.R. Alavi Moghaddam, M. Arami, Response surface optimization of Acid Red 119 Dye adsorption by mixtures of dried sewage sludge and sewage sludge ash, Clean Soil Air Water, 40 (2012) 652–660.

[22] C B. Wang, W.X. Zhang, Synthesizing nanoscale iron particles for rapid and complete dechlorination of TCE and PCBs, Environ. Sci. Technol., 31 (1997) 2154–2156.

[23] R. Rakhshaee, Rule of Fe^0 nano-particles and biopolymer structures in kinds of the connected pairs to remove Acid Yellow 17 from aqueous solution: simultaneous removal of dye in two paths and by four mechanisms, J. Hazard. Mater., 197 (2011) 144–152.

[24] N. Goldstein, F.L. Greenlee, Influence of synthesis parameters on iron nanoparticle size and zeta potential, J. Nanopart. Res., 14 (2012) 760.

[25] N. Efecan, T. Shahwan, A.E. Ero◎lu, I. Lieberwirth, Characterization of the uptake of aqueous Ni^{2+} ions on nanoparticles of zero-valent iron (nZVI), Desalination, 249 (2009) 1048–1054.

[26] C. Zhang, Z. Zhu, H. Zhang, Z. Hu, Rapid decolorization of Acid Orange II aqueous solution by amorphous zero-valent iron, J. Environ. Sci., 24 (2012) 1021–1026.

[27] P. Li, Y. Song, S. Wang, Z. Tao, S. Yu, Y. Liu, Enhanced decolorization of methyl orange using zero-valent copper nanoparticles under assistance of hydrodynamic cavitation, Ultrason. Sonochem., 22 (2015) 132–138.

[28] Y. He, J.F. Gao, F.Q. Feng, C. Liu, Y.Z. Peng, S.Y. Wang, The comparative study on the rapid decolorization of azo, anthraquinone and triphenylmethane dyes by zero-valent iron, Chem. Eng. J., 179 (2012) 8–18.

[29] K.B. Tan, M. Vakili, B.A. Horri, P.E. Poh, A.Z. Abdullah, B. Salamatinia, Adsorption of dyes by nanomaterials: recent developments and adsorption mechanisms, Sep. Purif. Technol., 150 (2015) 229–242.

[30] Z.X. Chen, X.Y. Jin, Z. Chen, M. Megharaj, R. Naidu, Removal of methyl orange from aqueous solution using bentonite-supported nanoscale zero-valent iron, J. Colloid Interface Sci., 363 (2011) 601–607.

[31] Y.T. Lin, C.H. Weng, F.Y. Chen, Effective removal of AB24 dye by nano/micro-size zero-valent iron, Sep. Purif. Technol., 64 (2008) 26–30.

[32] S.H. Chang, S.H. Chuang, H.C. Li, H.H. Liang, L.C. Huang, Comparative study on the degradation of I.C. Remazol Brilliant Blue R and I.C. Acid Black 1 by Fenton oxidation and Fe^0/air process and toxicity evaluation, J. Hazard. Mater., 166 (2009) 1279–1288.

[33] X. Jin, Z. Chen, Z. Chen, R. Zhou, Synthesis of kaolin supported nanoscale zero-valent iron and its degradation mechanism of Direct Fast Black G in aqueous solution, Mater. Res. Bull., 61 (2015) 433–438.

[34] J. Fan, Y. Guo, J. Wang, M. Fan, Rapid decolorization of azo dye methyl orange in aqueous solution by nanoscale zerovalent iron particles, J. Hazard. Mater., 166 (2009) 904–910.

[35] W.J. Liu, T.T. Qian, H. Jiang, Bimetallic Fe nanoparticles: recent advances in synthesis and application in catalytic elimination of environmental pollutants, Chem. Eng. J., 236 (2014) 448–463.

[36] R.K. Gautam, V. Rawat, S. Banerjee, M.A. Sanroman, S. Soni, S.K. Singh, M.C. Chattopadhyaya, Synthesis of bimetallic Fe–Zn nanoparticles and its application towards adsorptive removal of carcinogenic dye malachite green and Congo red in water, J. Mol. Liq., 212 (2015) 227–236.

[37] S. Wei, H. Ren, J. Li, J. Shi, Z. Shao, Decolorization of organic dyes by zero-valent iron in the presence of oxalic acid and influence of photoirradiation and hexavalent chromium, J. Mol. Catal. A: Chem., 379 (2013) 309–314.

[38] K. Yetilmezsoy, A. Saral, Stochastic modeling approaches based on neural network and linear-nonlinear regression techniques for the determination of single droplet collection efficiency of countercurrent spray towers, Environ. Model. Assess., 12 (2007) 13–26.

[39] D.P. Haaland, Experimental Design in Biotechnology, Marcel Dekker Inc., New York, 1999.

[40] Z. Ayazi, Z.M. Khoshhesab, S. Norouzi, Modeling and optimizing of adsorption removal of Reactive Blue 19 on the magnetite/graphene oxide nanocomposite via response surface methodology, Desal. Wat. Treat., 57 (2016) 25301–25316.

[41] M.R. Sohrabi, S. Amiri, H.R.F. Masoumi, M. Moghri, Optimization of Direct Yellow 12 dye removal by nanoscale zero-valent iron using response surface methodology, J. Ind. Eng. Chem., 20 (2014) 2535–2542.

[42] M. Gholinezhad, A.P. Zanganeh, M.R. Ramzanpour, A. Zamani, Optimization and response surface modeling of chromium removal from aqueous solution using nano zero valent ıron, Int. J. Agric. Innovations Res., 2 (2014) 2319–1473.

[43] M. Fan, T. Li, J. Hu, R. Cao, Q. Wu, X. Wei, L. Li, X. Shi, W. Ruan, Synthesis and characterization of reduced graphene oxide-supported nanoscale zero-valent ıron (nZVI/rGO) composites used for Pb(II) removal, Materials, 98 (2016) 687.

[44] Q.Z. Hong, G. Yang, Constructions of the general solution for of partial differential equations with variable coefficients, Appl. Math. Mech., 12 (1991) 149–153.

[45] Y. Lin, Z. Chen, Z. Chen, M. Megharaj, R. Naidu, Decoloration of acid violet red B by bentonite-supported nanoscale zero-valent iron: reactivity, characterization, kinetics and reaction pathway, Appl. Clay Sci., 93–94 (2014) 56–61.

[46] Y.P. Sun, X. Li, J. Cao, W. Zhang, H.P. Wang, Characterization of zero-valent iron nanoparticles, Adv. Colloid Interface Sci., 120 (2006) 47–56.

[47] R. Venkatapathy, D.G. Bessingpas, S. Canonica, J.A. Perlinger, Kinetics models for trichloroethylene transformation by zero-valent iron, Appl. Catal., B, 37 (2002) 139–159.

[48] F. Luo, D. Yang, Z. Chen, M. Megharaj, R. Naidu, The mechanism for degrading Orange II based on adsorption and reduction by ion-based nanoparticles synthesized by grape leaf extract, J. Hazard. Mater., 296 (2015) 37–45.